Supporting Information

Metzger et al. 10.1073/pnas.0911330107

SI Text

Methods. ***Environmental chamber.*** Several chamber experiments were carried out using SO_2 mixing ratios between 0 and 20 ppb and trimethylbenzene (TMB) mixing ratios of 70–1,200 ppb, while keeping other parameters, such as temperature, relative humidity (*RH*), TMB-NO_x-ratio virtually constant. Details of the indoor PSI chamber, the experimental setup and the instrumentation are described elsewhere (1). Briefly, photooxidation experiments were carried out in the 27-m^3 Teflon chamber (DuPont Teflon fluorocarbon film, FEP) at approximately 20 °C and $53 \pm 5\%$ *RH*. The chamber was first humidified before introducing NO, NO_2 and SO_2. A known amount of 1,3,5-trimethylbenzene (Fluka, 99.5%) was evaporated in a heated glass sampling bulb and flushed with pure air into the chamber where it was allowed to equilibrate for 30 min. Four xenon arc lamps (4 kW each) were used to simulate the solar light spectrum and start the photochemistry.

A SO_2 monitor (Monitor Labs 9850) was used to measure the input concentration of SO_2. A wet effluent diffusion denuder—aerosol collector (WEDD-AC) coupled to an ion chromatography—mass spectrometry (IC-MS) system was used to measure concentrations of organic and inorganic acids in the gas and aerosol phase as well as the initial gas-phase-concentration of SO_2 (2). The SO_2 is taken up by the denuder and rapidly oxidized to H_2SO_4. The sum of SO_4^{2-} and SO_3^{2-} measured in the denuder corresponds to the SO_2 ($+H_2SO_4$) concentration in the chamber, whereas particulate H_2SO_4 is measured in the aerosol collector. The resulting uncertainty in the SO_2 input concentration is conservatively estimated at about 50% and is considered in the error calculation of H_2SO_4.

TMB and its oxidation products were monitored using proton-transfer-reaction mass spectrometry (PTR-MS, Ionicon Analytik GmbH, Austria). The sensitivity of the instrument was determined using standards (Apel-Riemer Environmental Inc.; Denver, CO). For TMB an uncertainty of 5% was attributed to the data.

A condensation particle counter (CPC, model 3025, TSI Inc., USA) was used to monitor total particle number concentrations of particles with a minimum diameter of 3 nm. Number-weighted particle size distributions between 15 and 700 nm were obtained using a scanning mobility particle sizer (SMPS). The SMPS system consisted of a long column differential mobility analyzer (DMA, model 3071, TSI Inc., USA) and a TSI 3022 CPC. A "nano"-SMPS system, composed of a short DMA column and a TSI ultrafine water based condensation particle counter (UWCPC, Model 3786) was used to derive particle size distributions between 4 and 100 nm. Due to technical problems data are only available for a limited number of experiments. To reduce particle losses in the sampling lines the two SMPS systems and the CPC were mounted at the same inlet line close to the chamber. The measured size distributions were corrected for particle losses in the sample lines and for reduced CPC counting efficiency at small particle sizes prior to data analysis (1).

The aerosol mass produced (shown in Fig. 1, main text) is derived from measured number size distributions, assuming spherical shape and a density of 1.4 g cm^{-3} (3).

The CPC 3025 data were also corrected for particle losses in the sample lines and for reduced CPC counting efficiency at small particle sizes. If no size information was available from the nano-SMPS the number concentration in the diameter range of 3 to 15 nm particles, N_{3-15}, was estimated from the difference in the number concentration between the CPC and the SMPS integrated total. The mean diameter of the distribution, including the 3–15 nm size range, was then calculated and was used as a proxy for the size information needed.

Loss of particles to the chamber wall. The determination of the particle wall loss (*WL*) rate is based on the inverse-modeling procedure particle growth and nucleation (4) (PARGAN) (online version is available: http://iacweb.ethz.ch/php/pargan/), which is predicated on nonlinear regression analysis of the general dynamic equation (GDE) to fit the measured change of the aerosol size distribution due to wall losses, coagulation, and condensation.

It was shown in a number of studies that particle *WL* occurs as a result of Brownian diffusion and gravitational settling across a quasi-laminar layer adjacent to the chamber walls and thus depends on particle size (5–8). The first order rate constant for diffusional *WL*, $k_{\mathrm{wall,diff}}$, is proportional to the square root of the (size dependent) particle's Brownian diffusion coefficient, *D(r)* (5). Thus $k_{wall,\ diff}$ is given by

$$k_{wall,diff}(r) = C_{wall,diff}\sqrt{D(r)}, \qquad \textbf{[S1]}$$

where $C_{\mathrm{wall,diff}}$ is a proportionality constant in $cm^{-1}\ s^{-1/2}$. The value of $C_{\mathrm{wall,diff}}$ is dependent on the dimensions of the chamber and amount of mixing in the chamber. Its value has to be empirically determined by fitting the decay in particle concentration after nucleation has stopped.

The first order rate constant for *WL* by gravitational settling, k_{grav}, is given by

$$k_{wall,grav}(r) = m_{part}B(r)G\frac{S}{V}F_S, \qquad \textbf{[S2]}$$

where m_{part} is the particle mass, *B(r)* is the particle mobility, *G* is the acceleration by gravity (9.81 ms^{-2}), *S/V* is the surface to volume ratio of the chamber (0.02 cm^{-1}), and F_s is the ratio of the projected horizontal surface area to the total surface area in the chamber ($1/6 = 0.167$).

If the particle formation rate is zero (or as long as no particles grow into (or out of) the measured size range, i.e. as long as the particle growth does not influence their number) the decrease in particle number is caused by wall loss, dilution and coagulation, and can be described by summing up their contributions to each size bin in the GDE and integrating it over a certain time interval. The value of the proportionality factor, $C_{wall,diff}$, is then found by fitting the observed change in number (from 20 experiments typical values for $C_{wall,diff} = 0.013 \pm 45\%$ were found).

If $C_{wall,diff}$ and thus the overall (size dependent) wall loss rate is known, the measured size distribution can be corrected from the time of particle formation for the loss of particles to the walls.

Calculation of the H_2SO_4 and NucOrg concentrations. The concentration of H_2SO_4 and NucOrg in the chamber were calculated using a simple kinetic model by considering the relevant production and loss terms represented in Eq. **S3**. Wall loss (with rate constant k_{wall,H_2SO_4}) and condensation onto particles [with rate constant k_{cond,H_2SO_4} also called condensation sink, *CS* (9)] are the dominant sinks for condensable vapors like H_2SO_4.

$$\frac{d[H_2SO_4]}{dt} = k_{OH+SO_2}[OH][SO_2] - k_{dil}[H_2SO_4] - k_{wall,H_2SO_4}[H_2SO_4] - k_{cond,H_2SO_4}[H_2SO_4] \quad \textbf{[S3]}$$

The dilution rate (k_{dil}) (derived from the dilution flow divided by the chamber volume) is typically in the range of $5 \times 10^{-6} s^{-1}$ and negligible. k_{cond,H_2SO_4} is the (time-dependent) pseudo-first-order loss rate of H_2SO_4 due to condensation onto existing particles [i.e., also called the condensation sink (9)], calculated from the measured aerosol size distributions using the Fuchs-Sutugin equation (4).

The above described theory of particle losses in chambers can be extended to calculate wall deposition rates of molecular species (10). Thus the wall loss rate for H_2SO_4 was estimated using the same dependence as found for aerosol particles (4):

$$k_{wall,H_2SO_4} = C_{wall,diff}\sqrt{D}, \quad \textbf{[S4]}$$

where $C_{wall,diff}$ is derived from the observed aerosol wall loss and the H_2SO_4 diffusion coefficient is assumed to be 0.1 cm^2 s^{-1} (11, 12). This implicitly assumes that H_2SO_4 will always stick to the surface upon impact and that release from the surface to the gas phase after uptake does not occur (i.e., that the accommodation coefficient equals one) (10).

The wall loss rate and condensation sink for NucOrg are slightly smaller than the calculated rates of H_2SO_4 because of the larger molecular mass (assuming 200 amu). Thus $k_{wall;NucOrg} = k_{wall,H_2SO_4}/3$ and $CS_{NucOrg} = CS_{H_2SO_4}/3$ (13).

In the atmosphere, aerosol nucleation always competes with the uptake of condensable gases on the already existing aerosol particles. As there is no pre-existing aerosol present in our chamber the loss of H_2SO_4 to the wall competes with nucleation. It is of similar magnitude as the typical loss due to condensation during continental boundary layer nucleation events [e.g., 0.002 s^{-1} (14)].

Berndt et al. (15) hypothesized that SO_2 oxidation products other than H_2SO_4 (i.e., a peroxy type radical formed during the SO_2 oxidation) may be more efficient in producing particles than H_2SO_4 itself. A modeling analysis shows that under our conditions with high NO_x concentrations this formation is unlikely. However, the existence of such a formation pathway would not change our conclusions.

Uncertainty in the H_2SO_4 and NucOrg concentrations. The largest sources of uncertainty regarding the determination of the gas phase concentrations are the ill-defined wall loss rates of both H_2SO_4 and NucOrg. By assuming an accommodation coefficient ($\alpha_{H_2SO_4,Teflon}$) equal to one the upper limit of the H_2SO_4 wall loss is calculated (= base case). However accommodation coefficients for gases on Teflon walls are likely to be less than unity.

The uncertainties in the wall loss stemming from unknown accommodation effects are captured in a sensitivity study in order to investigate its influence on the concentrations of H_2SO_4 and NucOrg. The determined wall loss rate ($\alpha_{H_2SO_4,Teflon} = 1$) was lowered by a factor of 4 (arbitrarily) and 200 (assuming the same accommodation coefficient as found for HNO_3 on Teflon walls (10).

The results are shown in Fig. S4 for H_2SO_4 (*A*) and NucOrg (*B*) for experiments with different concentrations of SO_2 and TMB. The dashed lines show the concentration traces if wall loss and condensation onto particles is neglected. For the other cases wall loss and condensation onto particles was considered. The solid line represents the wall loss base case resulting in the lowest concentrations of H_2SO_4 or NucOrg. Reducing the wall loss rates (base) by a factor of 4 and 200 systematically shifts the calculated H_2SO_4 and NucOrg concentrations to higher values (up to 1 order of magnitude).

Assuming an accommodation coefficient of HNO_3 the concentrations are similar to the case if *WL* were completely neglected and thus can be regarded as the lowest (highly unrealistic) limit. At the beginning of an experiment, when no or only very small particles are present, *WL* is the dominant loss process for H_2SO_4. As soon as particles are formed condensation onto particles overcomes the *WL* and limits the H_2SO_4 or NucOrg concentration resulting in a strong dip in the concentration.

In summary: Reducing the *WL* by a factor of 200 would lead to:

- Increase of the threshold of the H_2SO_4 concentration when 3-nm particles start to appear from 5.0×10^6 to 3×10^7 molecules cm^{-3}.
- The H_2SO_4 concentrations in Fig. 2 would be shifted by about an order of magnitude to higher concentrations. However, since the *WL* does not vary in time, it merely serves as scaling factor and thus does not influence the dependency of the nucleation rate from H_2SO_4 and NucOrg.
- Condensation of H_2SO_4 may explain up to 70% of $GR_{1.5-3}$ if wall losses are neglected (Table S1).

Besides the uncertainty in the *WL* rates (due to unknown accommodation coefficients) the errors in the H_2SO_4 concentration was estimated to be 65%, assuming an uncertainty of the SO_2 input concentrations of 50%, an uncertainty of $C_{wall,diff}$, the condensation sink and the dilution rate of 50% each. An uncertainty of 15% is attributed to the reaction rates (TMB + OH and SO_2 + OH). In order to calculate the OH radical concentration the TMB decay had to be fitted to reduce noise in the derivation. The quality of the fit greatly affects the H_2SO_4 concentration calculated, but mainly in the beginning of the experiment. This was estimated to cause an additional 25% in the error.

Calculation of the particle formation rates (J_3, $J_{1.5}$) and $GR_{1.5-3}$. The formation rate of 3-nm particles, J_3, was deduced from the CPC data (5). J_3 is by definition the rate at which particles grow beyond 3 nm. This can be approximated by the measured rate of change in the CPC number concentration, dN_3/dt, correcting for other processes that influence the number concentration, such as coagulation, wall loss, and dilution:

$$J_3 = \frac{dN_3}{dt} + k_{coag}(r)(N_3(r))^2 + k_{wall}(r)N_3(r) + k_{dil}N_3(r), \quad \textbf{[S5]}$$

where N_3 is the number concentration of particles with diameter larger than 3 nm, as measured by the CPC. The dilution rate (k_{dil}) is independent of particle size. It is derived from the replenishment flow divided by the chamber volume and is typically in the range of 5×10^{-7} s^{-1} and thus negligible.

The wall loss rate constant (k_{wall}) is derived as discussed above. Typical wall loss rates for 3-, 10- or 50-nm particles are around 6×10^{-4}, 2×10^{-4}, and 4×10^{-5} s^{-1}. The wall loss rate is calculated based on the mean diameter from the SMPS and CPC. When no size information from the nano-SMPS is available and for times when the particles are below the size cut of the SMPS, k_{wall} is calculated for 6.7-nm particles (the log mean between 3 and 14 nm, $k_{wall} = 3 \times 10^{-4}$ s^{-1}). This would cause a factor of two error in the wall loss rate if all particles are close to 3 or 14 nm.

In the beginning of our experiments no pre-existing aerosol was present in the chamber thus coagulation scavenging–losses with larger sized particles–is negligible. During the initial nucleation most particles are of a similar size, and the effect of coagulation on J_3 can be approximated by (16)

$$(dN/dt)_{coag} = k_{coag}(N_3)^2, \quad \textbf{[S6]}$$

where N_3 is the number of particles and k_{coag} is the second order rate constant for coagulation of monodisperse aerosols. At each time step k_{coag} is estimated for particle sizes corresponding to the mean diameter determined from the SMPS. For times when the particles are below the size cut of the SMPS it is calculated for 6.7-nm particles. Calculation of J_3 is only affected at high particle loadings as typical coagulation rates are low: e.g., between 3-nm particles or between 3- and 20-nm particles they are in the range of 10^{-9} and 10^{-8} s^{-1}.

We define Δt as the time that the particles spend growing from their nucleating cluster (assumed to be 1.5 nm, at time t) to a size where they can be measured (3 nm, at time t'). Then the growth rate from 1.5 to 3 nm ($GR_{1.5-3}$) can be expressed as

$$GR_{1.5-3} = \frac{1.5\ nm}{\Delta t}. \qquad \textbf{[S7]}$$

The $GR_{1.5-3}$ values (in nm h^{-1}) were estimated from the time delays between the rise in H_2SO_4 and the rise in J_3. A similar method has been used by e.g., refs. 17–19).

The atmospheric nucleation rate $J_{1.5}$ at time $t = t' - \Delta t$ was estimated from the J_3 values by integrating the loss processes (coagulation, wall loss, dilution) that have occurred between time of formation and time of measurement (20).

$$J_{1.5}(t) = J_3(t') \exp[\gamma \frac{CS'}{GR_{1.5-3}} (\frac{1}{1.5nm} - \frac{1}{3nm})] \qquad \textbf{[S8]}$$

Here CS' is the "reduced condensation sink" (in m^{-2}) and γ is a coefficient with a value of approximately 0.23 m^2 nm^2 h^{-1}. Under atmospheric conditions CS' describes coagulation scavenging whereas here also wall loss is included. The times t and t' are related as $t = t' - \Delta t$, where Δt = 1.5 nm/$GR_{1.5-3}$. This equation was applied in a running window $[t, t' + \Delta t]$ throughout each analyzed experiment. For $GR_{1.5-3}$ and t' we used the fitted time delay estimate from the time delays between the rise in H_2SO_4 and the rise in J_3, and for CS' the median value from the interval $[t, t' + \Delta t]$. A similar expression connecting $J_{1.5}$ and J_3 has recently been used by (21 and references therein) using a slightly different notation.

The macroscopic particle growth rate (dD_p/dt, nm h^{-1}) can be estimated directly from the temporal evolution of the mean ($D_{p,mean}$) and modal ($D_{p,modal}$) diameter of the nucleation mode. To determine the modal diameter, the size distributions were parameterized by a least square log-normal fitting, yielding the parameters of the log-normal modes.

The growth rate can be related to the concentration of the condensing species by

$$\frac{dD_p}{dt} = \frac{2m_v\beta_m DC}{D_p\rho}, \qquad \textbf{[S9]}$$

where D_p is the particle diameter, m_v is the molecular mass of condensable vapor, β_m is the transitional correction factor of mass flux, D is the diffusion coefficient and ρ is the particle density (5). C is defined as the difference between the actual and the saturation concentration. Note that the relation between growth rate and vapor concentration depends on assumptions of the properties of the condensable vapor, such as molecular mass (assumed to be 200 amu for organics), diffusion coefficient and mass accommodation coefficient (α = 1).

The fraction of growth rate $GR_{1.5-3}$ that could be explained by the condensation of H_2SO_4 can be estimated by comparing the measured $GR_{1.5-3}$ to the growth rate calculated from the H_2SO_4 concentration, using Eq. **S9**. However this equation is derived for spherical nucleation mode particles from macroscopic condensation theory, and these assumptions do not hold anymore for 1.5–-3-nm sized particles. Condensation is enhanced at these small particle sizes compared with the macroscopic treatment by as much as a factor of 2–3 (22, 23). Therefore the contribution of H_2SO_4 to the growth rate was calculated according to Eq. **S9** with a condensation enhancement factor of 2.5. It can thus be understood as an upper limit of the contribution of H_2SO_4 to the overall growth.

Modeling. The GLOMAP aerosol microphysics model was used to simulate the impact of different nucleation mechanisms on atmospheric aerosol. The GLOMAP model is an extension to the TOMCAT 3D global chemical transport model (24) and has been described in detail elsewhere (25, 26). Here we run the model with a horizontal resolution of 2.8° x 2.8° and 31 vertical levels between the surface and 10 hPa. The model is forced by European Centre for Medium-Range Weather Forecast (ECMWF) analyses. GLOMAP includes sulfate (*SU*), sea salt (*SS*), elemental carbon (*EC*), and organic carbon (*OC*) aerosol components. We treat two externally mixed distributions, each described by a two-moment sectional scheme with 20 sections spanning 3 nm to 10 μm dry diameter. One distribution, representing freshly emitted primary carbonaceous aerosol, contains *OC* and *EC*, is treated as hydrophobic and is not wet scavenged. The other distribution contains *SU*, *SS*, *EC*, and *OC*, is hydrophilic and is wet scavenged. Hydrophobic particles age to become hydrophilic through condensation of soluble gas-phase species and coagulation with hydrophilic particles. Aerosol and aerosol precursor emission are as described in Spracklen et al. (27). All model simulations have the same description of primary particle emissions (27). We assume that the first-stage oxidation products of monoterpenes form hydrophilic secondary organic aerosol (*SOA*) with a yield of 13% (27). We ran six different simulations with different descriptions of particle formation:

1. Binary homogeneous nucleation of H_2SO_4-H_2O (BHN) using the parameterization of Kulmala et al. (28).
2. Traditional cluster activation scheme (29) implemented throughout the atmospheric column ($J_{1.5}$ = 5x10^{-7} s^{-1}[H_2SO_4]).
3. Traditional cluster activation scheme restricted to the model boundary layer (BL) and at higher levels the BHN rate of Kulmala et al., (28) is used. This is the model setup that is described in detail in Spracklen et al. (27).
4. Traditional kinetic nucleation involving only sulfuric acid (30) implemented throughout the atmospheric column ($J_{1.5}$ = 4 x 10^{-13} cm^3 s^{-1}[H_2SO_4]^2).
5. Traditional kinetic nucleation involving only sulfuric acid (30) restricted to the BL and at higher levels the BHN rate of Kulmala et al. (31).
6. Binary homogeneous nucleation of H_2SO_4-H_2O and kinetic activation involving organics implemented throughout the atmospheric column. The formation rate of molecular clusters is calculated according to Eq. **5** using a prefactor of 5 x 10^{-13} cm^3 s^{-1}. We assume that the organic vapor in Eq. **5** can be represented by the first stage oxidation products of monoterpenes.

We compared simulated total aerosol number concentrations with observations made during the INTEX-NA experiment, which occurred over North America during July–August 2004 (31). In Fig. 3 (main text) we show the average of all observations made during the campaign over two different domains; the continental United States (28–53°N, 240–269°E) and US outflow (32–52°N, 290–323°E). We averaged all the available observations in each region to a 1-km altitude resolution and ran the model for the same period and averaged over the same domain as the observations.

Fig. 4 (main text) shows simulated surface mean particle number concentrations for these different simulations during spring-

time (April). Fig. S3 shows the ratios of simulated particle number between the different simulations. Over oceans sulfuric acid will be the dominant contributor to growth. In regions of continental outflow there are condensable organics resulting in simulated particle formation.

Discussion. ***Further insights into SOA formation and SOA yield-macroscopic particle growth.*** Insights into the general mechanism of SOA formation and growth kinetics is gained by plotting the amount of SOA formed per hydrocarbon reacted, known as growth curves (32). Fig. S5 A shows the time dependent growth curves from TMB photo-oxidation in the presence of different amounts of SO_2. The amount of TMB reacted at the time of nucleation decreases with increasing SO_2 mixing ratio (see Table S1). In the presence of SO_2, nucleation occurs earlier (Fig. 1, main text), but there is only little build-up of SOA mass in the early stages of these experiments. The SOA yield is practically the same for the different experiments suggesting that the most abundant condensing product is produced by the TMB oxidation (Fig. S5*B*). The mass of aerosol formed when $TMB_{reacted}$ below approximately 450 $\mu g/m^3$ is substantially higher in the presence of SO_2 (Fig. S5*A*). This could be explained by the earlier presence of nuclei (due to the earlier nucleation induced by H_2SO_4 – NucOrg clusters) providing the surface for condensable species to condense on. If there is no "seed aerosol", SOA formation is suppressed until the NO concentration approaches zero. Therefore part of the organic vapors might be lost to the chamber wall, until nucleation starts, reducing the yield in the early stages (33–35).

In a number of studies it was shown that the SOA formation (yield) is considerably enhanced in the presence of acidic seed aerosol (acidity through presence of H_2SO_4) (e.g., for isoprene and α-pinene [36, 37)], either through direct formation of organo-sulfates (38) or by enhancing aerosol phase reactions such as oligomerisation (39). As shown in Fig. S5 we found no evidence of higher SOA yields in the presence of SO_2 and thus H_2SO_4 acidity.

Fig. S5*C* shows the derived (macroscopic, >15 nm) *GR* for the five experiments shown in Fig. 1 (main text). *GRs* correlate negatively with SO_2. The negative correlation with SO_2 is heavily influenced by the fact that SO_2 determines the number concentration *N* of particles so strongly, and *GRs* correlates negatively with *N* because the particles act as a sink for the condensing vapor. As discussed in the main text, H_2SO_4 can explain up to 20% of the $GR_{1.5-3}$ (or up to 70% if wall loss were neglected). However, its contribution to the growth above 15 nm is typically less than 5%. Therefore, we can estimate the condensable vapor concentrations from the observed growth rates of the aerosol size distribution (e.g., organic vapors that participated in SOA formation; $C\text{-}C_{sat}$, Eq. **S9**; MW $200g/\mathrm{mol}$, and $\alpha = 1$).

The vapor concentration needed to initiate nucleation depends on the H_2SO_4 concentration. Without any SO_2 (or H_2SO_4) about three times more organic vapor is needed to start new particle formation. Even with 0.4 ppb SO_2 the needed organic vapor concentration is clearly higher than for larger SO_2 concentrations. The high concentration required for the organics to nucleate without sulfuric acid shows that new particle formation from those organic compounds by themselves is implausible under atmospherically relevant concentrations.

1. Paulsen D, et al. (2005) Secondary organic aerosol formation by irradiation of 1,3, 5-trimethylbenzene-NO_x-H_2O in a new reaction chamber for atmospheric chemistry and physics. *Environ Sci Technol* 39(8):2668–2678.
2. Gaeggeler K, et al. (2008) Residential wood burning in an Alpine valley as a source for oxygenated volatile organic compounds, hydrocarbons and organic acids. *Atmos Environ* 42(35):8278–8287.
3. Alfarra MR, et al. (2006) A mass spectrometric study of secondary organic aerosols formed from the photooxidation of anthropogenic and biogenic precursors in a reaction chamber. *Atmos Chem Phys* 6:5279-5293.
4. Verheggen B and Mozurkewich M. (2006) An inverse modeling procedure to determine particle growth and nucleation rates from measured aerosol size distributions. *Atmos Chem Phys* 6:2927–2942.
5. Crump JG and Seinfeld JH (1981) Turbulent deposition and gravitational sedimentation of an aerosol in a vessel of arbitrary shape. *J Aerosol Sci* 12(5):405–415.
6. Crump JG, Flagan RC, and Seinfeld JH (1983) Particle wall loss rates in vessels. *Aerosol Sci Tech* 2(3):303–309.
7. McMurry PH and Rader DJ (1985) Aerosol wall losses in electrically charged chambers. *Aerosol Sci Tech* 4(3):249–268.
8. Park SH, Kim HO, Han YT, Kwon SB, and Lee KW (2001) Wall loss rate of polydispersed aerosols. *Aerosol Sci Tech* 35(3):710–717.
9. McMurry PH and Grosjean D (1985) Gas and aerosol wall losses in teflon film chambers. *Environ Sci Technol* 19(12):1176–1182.
10. Kulmala M, et al. (2001) On the formation, growth and composition of nucleation mode particles. *Tellus B* (53) 4:479–490
11. Pöschl U, et al. (1998) Mass accommodation coefficient of H_2SO_4 vapor on aqueous sulfuric acid surfaces and gaseous diffusion coefficient of H_2SO_4 in N_2/H_2O. *J Phys Chem A* 102(49):10082–10089.
12. Hanson DR and Eisele F (2000) Diffusion of H_2SO_4 in humidified nitrogen: Hydrated H_2SO_4. *J Phys Chem A* 104(8):1715–1719.
13. Bonn B, Kulmala M, Riipinen I, Sihto SL, and Ruuskanen TM (2008) How biogenic terpenes govern the correlation between sulfuric acid concentrations and new particle formation. *J Geophys Res-A* 113:D12
14. Dal Maso M, et al. (2002) Condensation and coagulation sinks and formation of nucleation mode particles in coastal and boreal forest boundary layers. *J Geophys Res-A* 107, doi: 10.1029/2001JD001053.
15. Berndt T, et al. (2008) SO_2 oxidation products other than H_2SO_4 as a trigger of new particle formation. Part 1: Laboratory investigations. *Atmos Chem Phys* 8(21):6365–6374.
16. Verheggen B and Mozurkewich M (2002) Determination of nucleation and growth rates from observation of a SO_2 induced atmospheric nucleation event. *J Geophys Res-A* 107, doi: 10.1029/2001JD000683.
17. Weber RJ, et al. (1997) Measurements of new particle formation and ultrafine particle growth rates at a clean continental site. *J Geophys Res-Atmos* (102) D4: 4375–4385.
18. Sihto SL, et al. (2006) Atmospheric sulphuric acid and aerosol formation: Implications from atmospheric measurements for nucleation and early growth mechanisms. *Atmos Chem Phys* 6:4079–4091.
19. Fiedler V, et al. (2005) The contribution of sulphuric acid to atmospheric particle formation and growth: A comparison between boundary layers in Northern and Central Europe. *Atmos Chem Phys* 5:1773–1785.
20. Kerminen VM and Kulmala M (2002) Analytical formulae connecting the "real" and the "apparent" nucleation rate and the nuclei number concentration for atmospheric nucleation events. *J Aerosol Sci* (33) 4:609–622.
21. Kuang C, McMurry PH, McCormick AV, and Eisele FL (2008) Dependence of nucleation rates on sulfuric acid vapor concentration in diverse atmospheric locations. *J Geophys Res-Atmos* D10209, doi: 10.1029/2007JD009253.
22. Lehtinen KEJ and Kulmala M (2003) A model for particle formation and growth in the atmosphere with molecular resolution in size. *Atmos Chem Phys* 3:251–257.
23. Korhonen H, Lehtinen KEJ, and Kulmala M (2004) Multicomponent aerosol dynamics model UHMA: model development and validation. *Atmos Chem Phys* 4:757-771.
24. Chipperfield MP (2006) New version of the TOMCAT/SLIMCAT off-line chemical transport model: Intercomparison of stratospheric tracer experiments. *Q J RoyMeteor Soc* 132(617):1179–1203.
25. Spracklen DV, et al. (2008) Contribution of particle formation to global cloud condensation nuclei concentrations. *Geophys Res Lett* 35, L06808, doi: 10.1029/2007GL033038.
26. Spracklen DV, Pringle KJ, Carslaw KS, Chipperfield MP, and Mann GW (2005) A global off-line model of size-resolved aerosol microphysics: I Model development and prediction of aerosol properties. *Atmos Chem Phys*5:2227–2252.
27. Spracklen DV, et al. (2006) The contribution of boundary layer nucleation events to total particle concentrations on regional and global scales. *Atmos Chem Phys* 6:5631–5648.
28. Kulmala M, Laaksonen A, and Pirjola L (1998) Parameterizations for sulfuric acid/water nucleation rates. *J Geophys Res-A* 103(D7):8301–8307.
29. Kulmala M, Lehtinen KEJ, and Laaksonen A (2006) Cluster activation theory as an explanation of the linear dependence between formation rate of 3 nm particles and sulphuric acid concentration. *Atmos Chem Phys* 6:787–793.
30. McMurry PH and Friedlander SK (1979) New particle formation in the presence of an aerosol. *Atmos Environ* 13 (12):1635–1651.
31. Singh HB, Brune WH, Crawford JH, Jacob DJ, and Russell PB (2006) Overview of the summer 2004 intercontinental chemical transport experiment-North America (INTEX-NA). *J Geophys Res-A* 111, D24S01, doi: 10.1029/2006JD007905.
32. Ng NL, et al. (2006) Contribution of first- versus second-generation products to secondary organic aerosols formed in the oxidation of biogenic hydrocarbons. *Environ Sci Technol* 40(7):2283–2297.
33. Pathak RK, et al. (2007) Ozonolysis of alpha-pinene: Parameterization of secondary organic aerosol mass fraction. *Atmos Chem Phys* 7(14):3811–3821.
34. Kroll JH, Chan AWH, Ng NL, Flagan RC, and Seinfeld JH (2007) Reactions of semivolatile organics and their effects on secondary organic aerosol formation. *Environ Sci Technol* 41(10):3545–3550.
35. Chan AWH, Kroll JH, Ng NL, and Seinfeld JH (2007) Kinetic modeling of secondary organic aerosol formation: effects of particle- and gas-phase reactions of semivolatile products. *Atmos Chem Phys* 7:4135–4147.

36. Kleindienst TE, Edney EO, Lewandowski M, Offenberg JH, and Jaoui M (2006) Secondary organic carbon and aerosol yields from the irradiations of isoprene and alpha-pinene in the presence of NO_x and SO_2. *Environ Sci Technol* 40(12):3807–3812.
37. Surratt JD, et al. (2007) Effect of acidity on secondary organic aerosol formation from isoprene. *Environ Sci Technol* 41(15):5363–5369.
38. Surratt JD, et al. (2007) Evidence for organosulfates in secondary organic aerosol. *Environ Sci Technol* 41(2):517–527.
39. Gao S, et al. (2004) Particle phase acidity and oligomer formation in secondary organic aerosol. *Environ Sci Technol* 38(24):6582–6589.

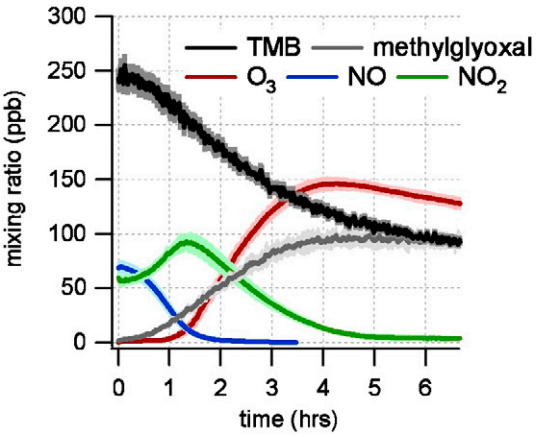

Fig. S1. Typical evolution of the major gas phase species for five individual experiments with similar initial concentrations of TMB and NO_x but SO_2 mixing ratios varying between 0 to 20 ppb (Fig. 1, main text). The experiment to experiment variability is indicated by the shaded area. The repeatability of the 5 independent experiments is excellent. The reaction of OH with TMB leads to formation of RO_2 radicals, which rapidly convert NO to NO_2. Ozone is formed from the photolysis of NO_2, and its concentration increases rapidly after *NO* concentration has dropped below 5 ppb. Methylglyoxal, a major primary oxidation product, is formed slowly in the beginning and increases more pronounced concurrent with TMB reacting away. A clear increase in particle number concentration is observed with increasing SO_2 mixing ratio whereas the overall gas phase chemistry is unaffected.

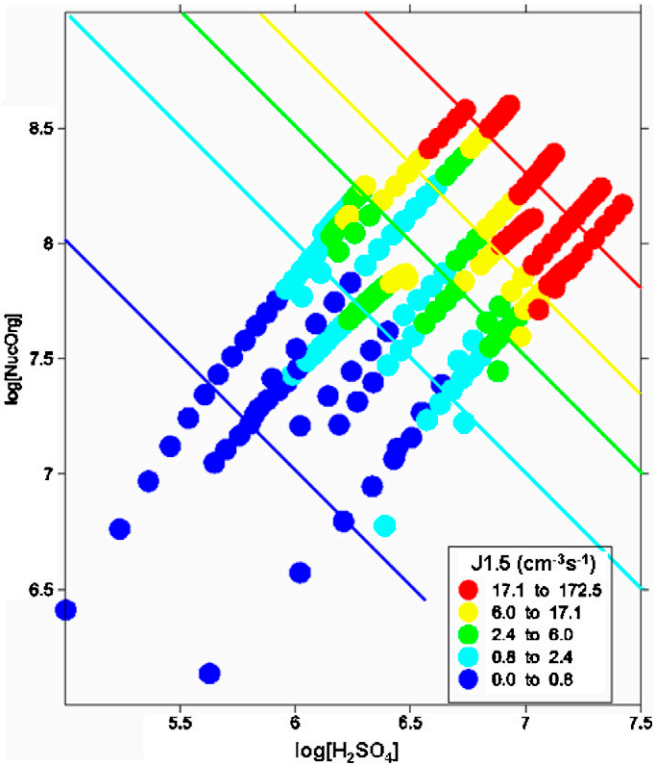

Fig. S2. Isopleth plot of $J_{1.5}$ (cm^{-3} s^{-1}) as a function of log[H_2SO_4] versus log[NucOrg]. The iso-lines are drawn to guide the eye. If $J_{1.5}$ depended on either H_2SO_4 or NucOrg alone the iso-lines would need to be horizontally or vertically, respectively. The diagonal iso-lines clearly show that our data can only be explained with a dependence of $J_{1.5}$ from both H_2SO_4 and NucOrg.

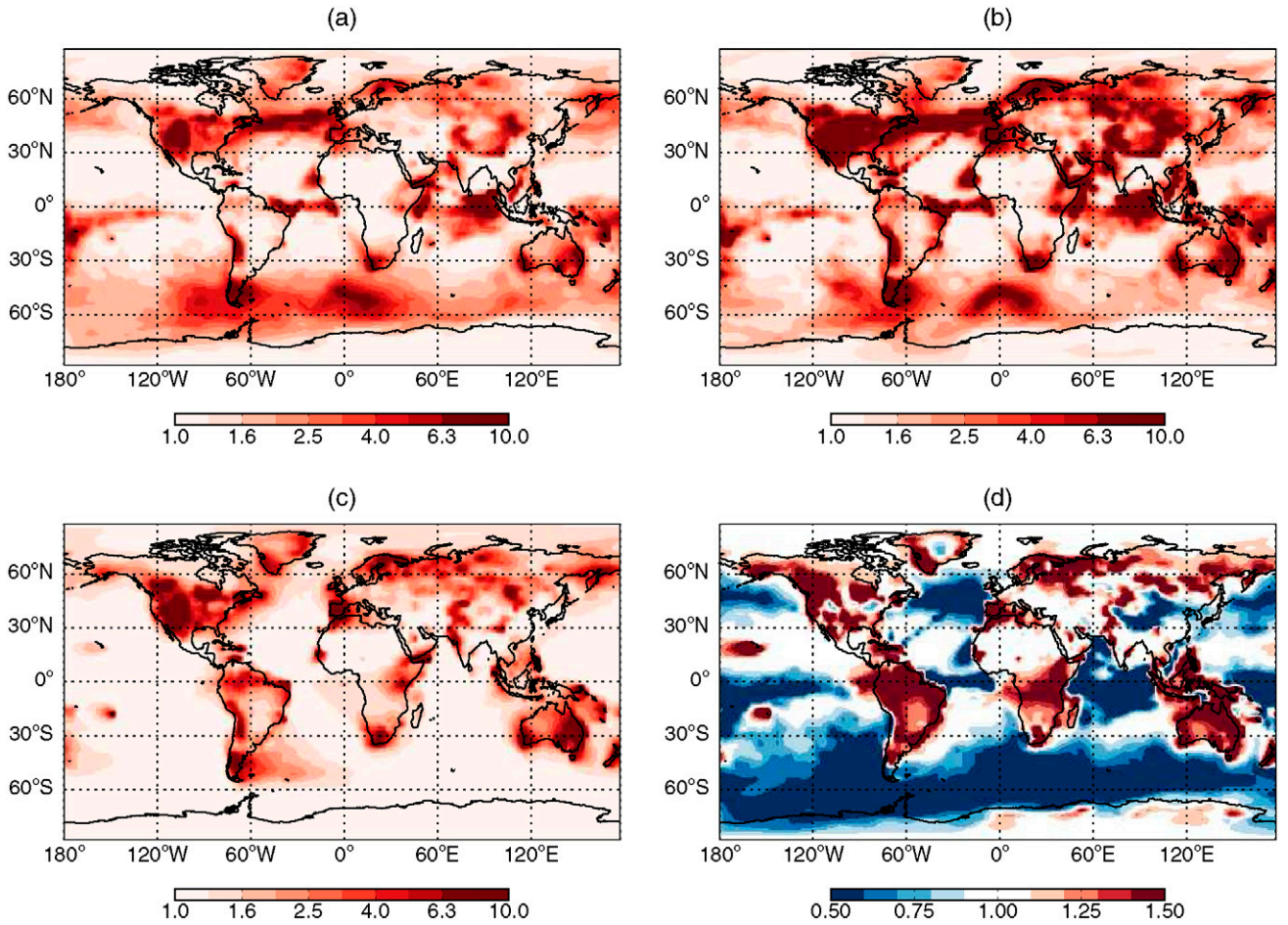

Fig. S3. Ratios of April surface mean total particle number concentrations (D_p > 3 nm) simulated using different nucleation mechanisms: (*a*) Activation mechanism restricted to the BL only (simulation 3): binary homogeneous nucleation (BHN, simulation 1); (*b*) Kinetic mechanism restricted to the BL only (simulation 5): simulation 1; (*c*) Kinetic nucleation involving organics (simulation 6): simulation 1; (*d*) simulation 6: simulation 3.

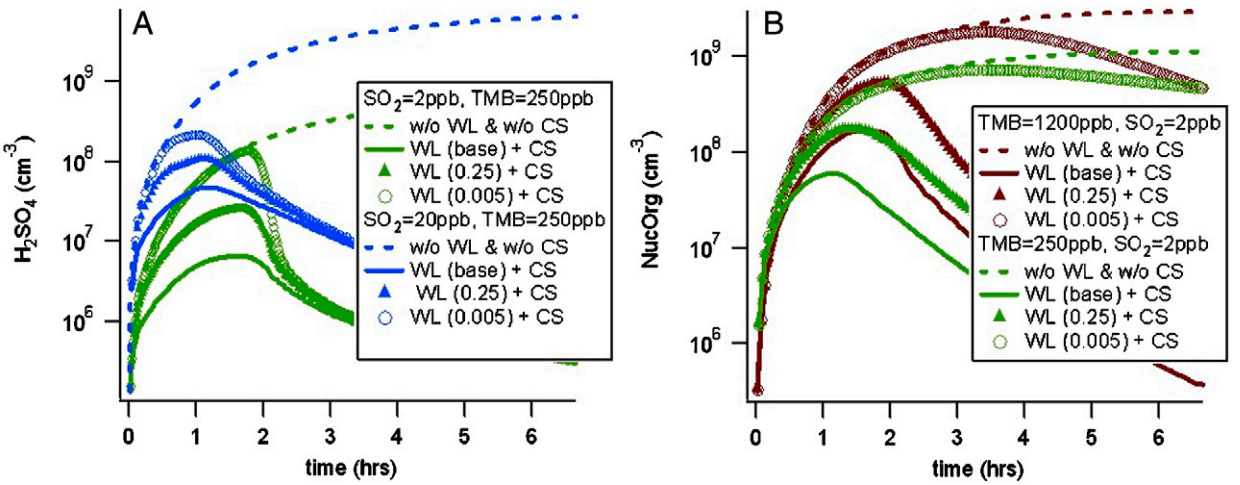

Fig. S4. Effect of the assumed wall loss rates on the concentrations of H_2SO_4 and NucOrg. The base case assumes that the wall loss is limited only by diffusion, with a mass accommodation coefficient (α) of unity (highest possible α and therefore lowest possible H_2SO_4 concentrations). In order to test the sensitivity the gas phase wall loss rates were reduced by a factor of 4 and by a factor of 200 which systematically shifts the calculated H_2SO_4 and NucOrg concentrations to higher values (up to 1 order of magnitude). The factor of 200 is in accordance with the reported wall loss rate of HNO_3 in smog chambers (i.e., α = 0.005). At the beginning of an experiment, when no or only very small particles are present, wall loss is the dominant loss process for H_2SO_4 and NucOrg. As soon as particles are formed condensation onto particles overcomes the wall loss and limits the H_2SO_4 and NucOrg concentrations resulting in a strong decrease in the concentration.

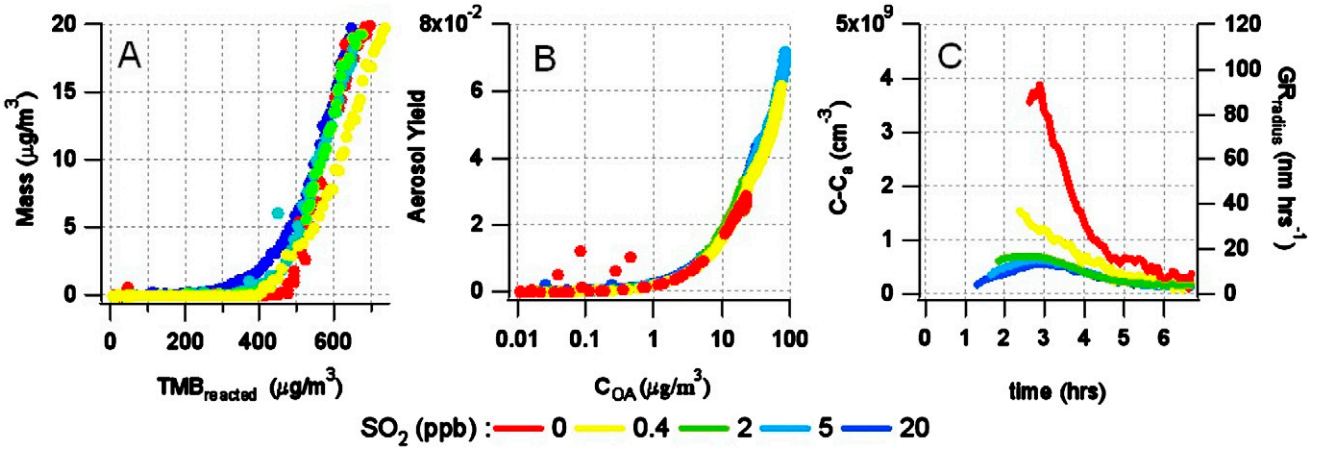

Fig. S5. (*A*) Influence of SO_2 on the real time aerosol yield: comparison of aerosol mass as a function of TMB reacted (growth curve). (*B*) Real-time aerosol yield as a function of aerosol mass concentration C_{OA}. (*C*) Time dependence of the radius growth rate (GR) and corresponding condensable vapor concentration ($C\text{-}C_{sat}$). With a lower SO_2 mixing ratio, a higher concentration of low vapor pressure organics needs to build up before nucleation kicks in. Initial mixing ratios: 250 ppb for TMB and 0–20 ppb for SO_2.

Table S1. Concentrations of $TMB_{reacted}$, H_2SO_4, and NucOrg at the time of particle appearance (ToPA) for a selection of experiments with similar initial TMB (experiments shown in Fig. 1, main text) or similar initial SO_2 mixing ratios

TMB (ppb)	SO_2(ppb)	Time* (min)	TMB reacted at ToPA (ppb±1σ)†	$GR_{1.5-3}$(nm/h)	Contribution of H_2SO_4 to $GR_{1.5-3}$ (%)	H_2SO_4 at ToPA (molecules/cm³)	NucOrg at ToPA (molecules/cm³)
Constant Organic							
250	0	124	72 ± 4	—	—	—	—
250	0.4	39	11 ± 3.5	2.4	8 (21; 42)	8.5E5 (2.3E6; 4.5E6)	1.7E7 (3.0E7, 4.0E7)
250	2	23	6.2 ± 4.7	4.3	8 (24; 47)	1.6E6 (4.6E6; 9.0E6)	8.0E6 (1.4E7,1.8E7)
250	5	21	5.5 ± 4.9	5	22 (58; 84)	5.0E6 (1.3E7; 1.9E7)	1.0E7 (1.4E7, 1.5E7)
250	20	9	3.3 ± 5.4	10	24 (44; 62)	1.1E7 (2.0E7; 2.8 E7)	8.0E6 (1.0E7,1.0E7)
Constant SO_2							
79	0.4	39	3 ± 4	2.3	7 (21, 48)	7.6E5 (2.2E6;5E6)	5.0E6 (1.0E7;1.3E7)
127	0.4	36	10 ± 4.7	2.5	11 (29; 52)	1.2E6 (3.3E6; 5.8E6)	1.4E7 (2.4E7;2.9E7)
250	0.4	37	11 ± 3.5	2.4	8 (21; 42)	8.5E5 (2.3E6; 4.5E6)	1.7E7 (3.0E7, 4.0E7)
603	0.4	36	16 ± 14	2.5	4 (12; 26)	5.0E5 (1.4E6;2.9E6)	2.6E7 (4.8E7; 6.4E7)

Also listed is the growth rate from 1.5 to 3 nm ($GR_{1.5-3}$) and the percentage contribution of H_2SO_4–$GR_{1.5-3}$.
Values in brackets show the sensitivity to changes in the assumed wall loss rate (rate reduced to 25% and 0.005%). The H_2SO_4/NucOrg concentration is described by production – loss. If the wall loss rate is overestimated the H_2SO_4/NucOrg concentration will be underestimated, especially for the experiments with lower SO_2 mixing ratios (more time passing before nucleation occurs and thus more time where loss processes affect the concentration).
*Time equals time of particle (>3 nm) appearance, ToPA, in minutes after the start of the experiment.
†Moving average over 15 min and standard deviation of this 15-min interval.